Viscous microstructural dampers with aligned holes: Design procedure including the edge correction

Dorel Homentcovschi[a)] and Ronald N. Miles
Department of Mechanical Engineering, SUNY Binghamton, New York 13902-6000

(Received 25 September 2006; revised 5 June 2007; accepted 12 June 2007)

The paper is a continuation of the works "Modelling of viscous damping of perforated planar micromechanical structures. Applications in acoustics" [Homentcovschi and Miles, J. Acoust. Soc. Am. **116**, 2939–2947 (2004)] and "Viscous Damping of Perforated Planar Micromechanical Structures" [Homentcovschi and Miles, Sensors Actuators, **A119**, 544–552 (2005)] where design formulas for the case of an offset (staggered) system of holes was provided. The present work contains design formulas for perforated planar microstructures used in MEMS devices (such as proof-masses in accelerometers, backplates in microphones, micromechanical switches, resonators, tunable microoptical interferometers, etc.) in the case of aligned (nonstaggered) holes of circular and square section. The given formulas assure a minimum total damping coefficient (including the *squeeze film damping* and the *direct* and *indirect* resistance of the holes) for an assigned open area. The paper also gives a simple edge correction, making it possible to consider real (finite) perforated planar microstructures. The proposed edge correction is validated by comparison with the results obtained by FEM simulations: the relative error is found to be smaller than 0.04%. By putting together the design formulas with the edge correction a simple integrated design procedure for obtaining viscous perforated dampers with assigned properties is obtained. © *2007 Acoustical Society of America.* [DOI: 10.1121/1.2756169]

PACS number(s): 43.38.Bs, 43.38.Kb [AJZ] Pages: 1556–1567

I. INTRODUCTION

Many microelectromechanical system (MEMS) devices include a plate that moves relative to a perforated stationary electrode, or backplate. The perforations in the backplate are often needed to reduce the time required to remove sacrificial materials between the moving structure and the backplate. In addition, the perforations are known to reduce viscous damping due to the squeezing of the air in the small space. Therefore, the study of a thin air layer being squeezed between a moving plate and a perforated backplate, referred as a planar microstructure, is important in many applications such as microphones, microaccelerometers, micromechanical switches, resonators, tunable microoptical interferometers, etc. Despite the large research effort dedicated to this subject, the elaboration of a simple design procedure for obtaining desired damping properties is still an open question. The primary aim of this paper is to describe such a design procedure including a practical approximate scheme to account for the change in damping due to the open edges of the structure.

Viscous damping is a critical factor for many MEMS transducers. Angular rate sensors require low damping in order to achieve sufficient sensitivity of the system under a given driving force in many applications. In the case of microphones (and also other sensors designed for small signal applications) the mechanical-thermal noise is often one of the limiting noise components. The magnitude of thermal noise depends only on temperature and the magnitude of mechanical damping.[1] Consequently, high viscous damping is associated also with large mechanical-thermal noise. If the damping is too low in a micromachined lateral accelerometer, the severe degree of resonance of the proof mass, upon an impact of external force, may produce a large signal that overloads the control circuitry, resulting in system failure. Many devices need to be damped for stable operation. Therefore, as was shown in Ref. 2, in designing a MEMS device, the consideration of viscous damping must be taken into account at the earliest stage. The efficient etching, the proper value of the viscous damping, and the control of the structure stiffness require a comprehensive understanding of the micromachined perforated systems and their dynamic behavior. Designers need insight into how to fine-tune the design parameters to achieve higher sensitivity and better overall performance.

The motion of the thin film of gas in a planar microstructure gives a squeezed-film damping that can adversely affect the dynamic response of the device.[3] There is an extensive literature dedicated to the study of the squeezed-film damping in MEMS (see Refs. 4–8, etc.). While the squeezed-film damping is reduced by the presence of the holes in one plate (or both plates), the vertical motion of the air within the holes gives a new viscous resistance, which adds to the squeezed-film damping. A rigorous analysis of the total damping problem requires the solution of the Navier-Stokes' system (or the simplified Stokes' approximation) in the 3-D domain composed of the space between the plates and holes. Unfortunately, as was shown in Ref. 9, the

[a)]Permanent address: University Politechnica of Bucharest, Applied Science Department and Institute of Mathematical Statistics and Applied Mathematics of Romanian Academy, Calea13 Septembrie #13, RO-76100, Bucharest, Romania. Electronic mail: homentco@binghamton.edu

 © 2007 Acoustical Society of America

full 3-D simulation of the Navier-Stokes system is practically impossible due to the huge number of elements needed. To simplify the problem an "*extended*" (modified) Reynolds' equation was formulated by Veijola and Matilla,[10] by adding an additional "*leakage*" term, due to perforations to the classical Reynolds' equation. The resulting equation was solved by using finite element method (FEM) tools by a homogenization method (where the leakage due to the holes is homogenized uniformly on the plate surface) in Refs. 11 and 12 and also by a different approach where the leakage is described as a spatially variable quantity (called by the author the Perforation Profile Reynolds' method).[13] Also, Bao *et al.* in Refs. 14 and 15 wrote a "*modified*" Reynolds' equation by adding to the classical equation a term related to the flow through holes. This partial differential equation (PDE) was integrated only in the case of a very long rectangular perforated plate by reducing it to an ordinary differential equation (ODE). Both the "*extended*" and the "*modified*" Reynolds' equations have the advantage of simultaneously taking into consideration both the presence of the holes and the finite edges of the damper. The drawbacks come from the fact that they are model equations (always involving a model error) that have to be solved numerically for each particular geometry of the perforated microstructure.

The two viscous effects, squeezed-film damping and the resistance of the holes, are not independent. In order to decrease the squeeze-film damping we have to "*drill*" more and more holes but each new hole adds its resistance to the total damping. In Refs. 16 and 17 approximate analytical expressions for the squeezed-film damping and the resistance of the holes were obtained for the particular case of infinite plates containing a regular, periodic, system of holes. By using these formulas the existence of an optimum number of perforations has been proved that minimizes the total viscous damping, giving an equilibrium between the two viscous components. Also, in the cited papers design formulas were given for the case of the offset (staggered) circular holes (when the domain of influence of a hole is a regular hexagon). The use of offset holes permits a better use of material, resulting in a smaller total pressure for a given amount of open area. However, in the case of offset holes we do not know a simple method to take into consideration the effect of the edges of finite plates.

In many MEMS applications employing planar microstructures it is common to use a regular system of aligned circular or square holes. In this case the domain of influence of a hole is a square. In this paper we first give design formulas for a perforated planar microstructure, which gives the minimum total damping for a given value of the area ratio, A (the ratio of the holes' area/total area of the plate). All these formulas prove true in the case of infinite planar microstructures. The advantage of the viscous dampers containing aligned holes is that in this case a simple method to introduce edge corrections can be developed. This can be accomplished simply by taking into consideration the change in squeezed-film damping for the cells next to the sides of the structures. This permits the design procedure to account for the real (finite) geometry of the perforated microstructure. The present work completes the previous papers in Refs. 16 and 17 by providing an integrated procedure for designing perforated dampers with assigned properties.

There is some misunderstanding of the combined effects of the squeeze film damping and the resistance of the holes. The determination of the squeeze film damping assumes a zero pressure condition along the edge of the hole. On the other hand, the flow through holes assumes a p_1 (nonzero) pressure boundary condition at the rim of the hole. In order to address this apparent incompatibility we introduced a section entitled "Squeeze film damping and resistance of the holes." While the squeeze film damping is obtained by solving a boundary value problem (BVP) with homogenous boundary conditions, the resistance of the holes has two components. These consist of a direct resistance of a hole F_d^h, which results from summing the tractions along the side surface of the cylindrical hole and an indirect resistance, denoted by F_i^h, which results from the change of the boundary condition along the rim of the hole from zero to the value p_1. The total resistance of a hole is the sum of the direct and indirect components. This is exactly the value of the resistance assumed in our previous papers (Refs. 16 and 17).

The indirect resistance of a hole is larger (in absolute value) than the direct resistance F_d^h; therefore any model of the flow in a perforated microstructure which considers only the direct resistance of holes is incomplete and may produce erroneous results.

In Sec. III we analyze the case of circular holes. Since in many applications the authors consider aligned square holes, formulas are given in Sec. IV for designing perforated microplanar structures with square holes giving the smallest damping coefficient [for a fixed area ratio (A)]. Section V is dedicated to the introduction of the edge correction. The idea is to modify the dimensions of the "*side*" cells such that the new cell has the same total pressure as the "*inner*" cells. In order to test how the correction works we considered a model structure with one-dimensional periodicity modified according to the introduced edge correction. The total pressure obtained by our procedure was compared with a FEM solution for the whole structure. For the whole domain of the parameter A the error resulting by using our correction is smaller than 0.04%. This numerically validates the introduced edge correction. The result of this analysis is that in the case of domains with the sides parallel to the coordinate axes, the design problem is a simple modification of that for infinite domains, the difference being the elimination in some cases of a line and/or a column of holes.

To keep the presentation simpler and at the same time to account for special effects we added a section that discusses the limits of applicability of given formulas and indicates the modifications imposed by different special conditions.

Section VII contains an example of the design procedure for a perforated planar microstructure given in the literature.

The advantage of the new procedure over the previous design methods is that instead of writing a new model PDE (which takes into consideration somehow the presence of the holes) and integrating this equation numerically for every specified structure, we give design formulas that provide the periodic structure having the smallest damping. Afterwards,

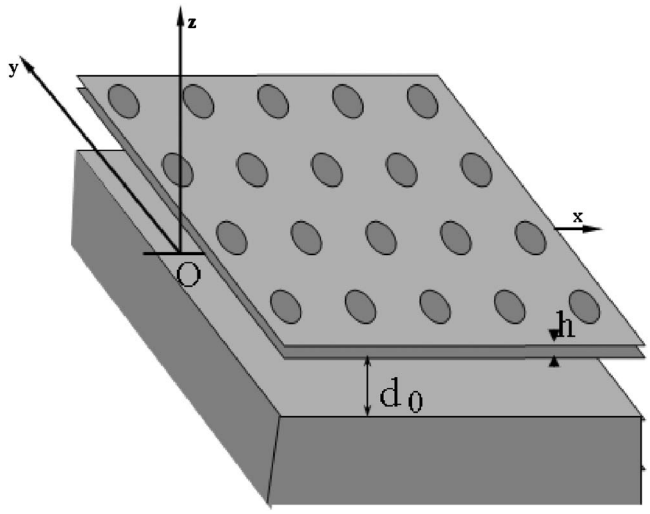

FIG. 1. A perforated planar microstructure with aligned holes.

the edge correction completes the design procedure by modifying only the dimension of the open side cells to account for the real (assigned) geometry of the damper.

II. THE SQUEEZE FILM DAMPING AND THE RESISTANCE OF HOLES

We consider the microstructure in Fig. 1 where the upper (mobile) plate has a regular system of cylindrical holes placed in the corners of a regular square web of period-d parallel to the coordinate axes Ox, Oy. Figure 2(a) shows a circular hole of radius r and domain of influence D. The union of the hole and of the domain D (called also a cell) is a square of side length d having the same center as the hole. In the cross-sectional view d_0 is the average gap between the diaphragm and counter electrode and h is the thickness of the backplate (also called the depth into the page).

A. The squeeze film damping

The Reynolds' equation, satisfied by the pressure $p(x,y)$ in the gap, yields Poisson's equation,[3–17]

$$\frac{\partial^2 p}{\partial x^2} + \frac{\partial^2 p}{\partial y^2} = \frac{12\mu}{d_0^3} w, \quad \text{in } D \tag{1}$$

where μ is the viscosity of the fluid between the plates and w is the velocity of the upper (mobile) plate. The PDE (1) has to be integrated subject to the following boundary conditions:

$$\frac{\partial p}{\partial n} = 0 \quad \text{along the square sides } C_N, \tag{2}$$

$$p(x,y) = 0 \quad \text{along the rim of the hole } C_0. \tag{3}$$

Once the pressure p is determined, the squeeze-film damping force F^s for the cell is defined by

$$F^s = -\int\int_D p(x,y)\, dx\, dy. \tag{4}$$

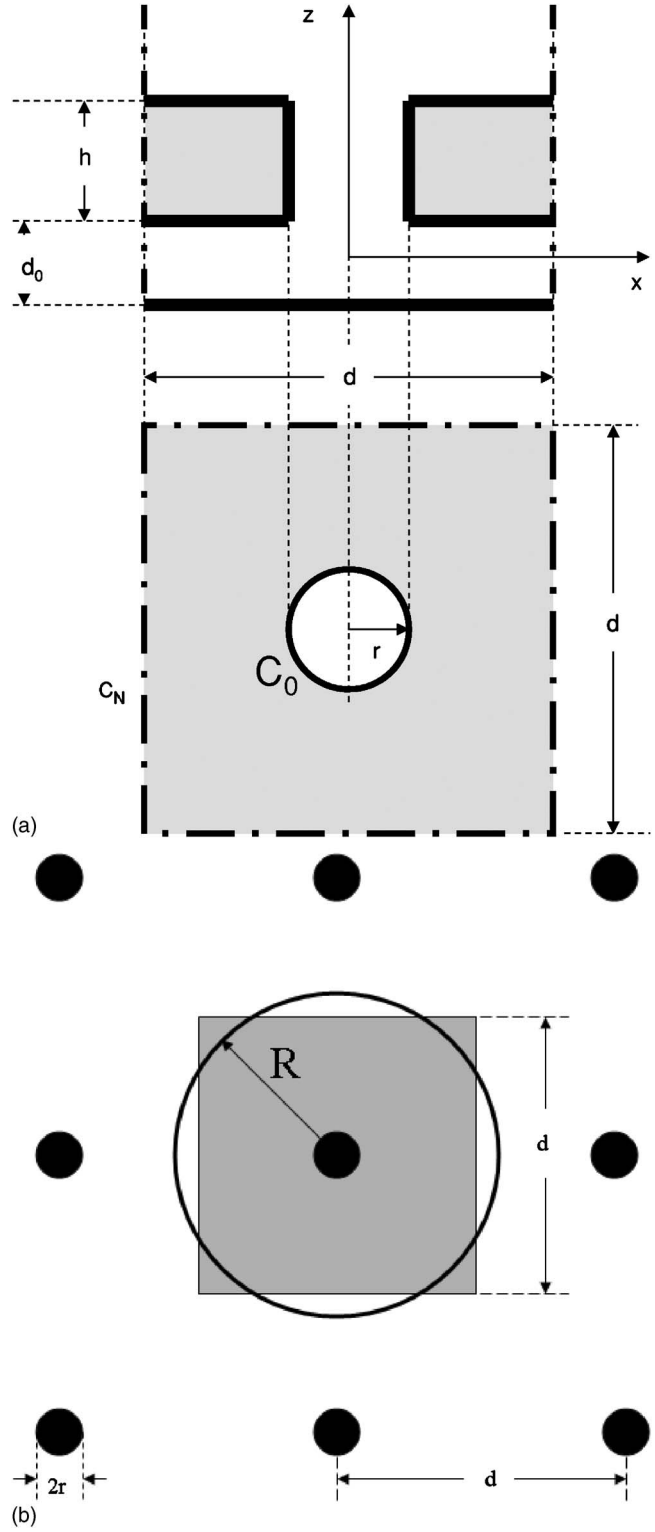

FIG. 2. (a) The cross-sectional view and the top view of a cell of the perforated microstructure with aligned circular holes. (b) The influence domain (the cell) of a circular hole and its circular approximation.

Equation (1) is valid in the case of incompressible fluids. Generally, the velocity of the mobile plate w is a function of x, y, and t. Consequently, a more rigorous approach given in Ref. 17 shows that on the left-hand side an inertial term has to be added. However, the analysis of Zuckerwar in Ref. 18

(reconsidered also in Ref. 19) shows that in the case of microphones, in the audio frequency domain the damping is practically independent of frequency.

The integration of Eqs. (1)–(3) can be performed by numerical methods using, for example, the software developed for solving steady state heat propagation problems. More analytical results can be obtained in the case where the velocity w is constant over the mobile plate (the piston problem). This is the case in many MEMS devices that employ a planar parallel-plate capacitor, in which one plate is actuated electrically and its motion is detected by capacitive changes. The pistonlike model of the moving diaphragm is applicable at sufficiently low frequencies where the amount of air displaced by the membranes rather than the exact shape of the moving surface is important in characterizing the device. Such an approximation is common in analyzing the behavior of microphones (see, for example, Ref. 19).

For obtaining a simple analytical solution, the external boundary of the cell (the square of d-side length) is substituted by a circle of radius $R=d/\sqrt{\pi}$ [Fig. 2(b)]. This way the problem becomes axially symmetric for an annulus of the same area as the domain D. In polar coordinates (ρ,θ) Eq. (1) becomes

$$\frac{1}{\rho}\frac{\partial}{\partial\rho}\left(\rho\frac{\partial p}{\partial\rho}\right)=\frac{12\mu}{d_0^3}w, \quad r<\rho<R,$$

and its solution satisfying the boundary conditions (2) and (3) is

$$p(\rho)=\frac{12\mu}{d_0^3}\left(\frac{\rho^2-r^2}{4R^2}-\ln\sqrt{\frac{\rho}{r}}\right)w. \tag{5}$$

Correspondingly, the squeeze-film damping force is given by substituting this expression for the pressure in formula (4). This leads to Ščvor's formula,[20]

$$F^s=\frac{12\pi\mu R^4}{d_0^3}C(A)\omega, \tag{6}$$

where $C(A)$ is given by

$$C(A)=A/2-A^2/8-0.25\ln A-3/8,$$

and the *area ratio* A is defined as the ratio of the area of a hole to the area of a cell,

$$A=\frac{\pi r^2}{\pi R^2}=\frac{\pi r^2}{d^2}. \tag{7}$$

Remark 1: The approximation of the cell by an annulus of the same area, suggested by Ščvor's approach, was performed in Refs. 3 and 16. *In Ref.* 17 *an analysis of the error involved in this approximation shows that formula* (6) *works well as long as* A<0.4. *A correction to this formula* (*presented in Sec.* VI C) *extends its validity until* $A=0.75$.

B. The resistance of holes

The other component of the viscous damping in a perforated microstructure, caused by the vertical motion of the fluid through the holes, is the holes' resistance denoted by F^h. For determining the resistance of holes, a hole in the lower plate is modeled as a circular pipe, of radius r and length h, and the fluid flow is assumed to be a Hagen-Poiseuille fully developed flow. The pressure along the upper edge of the hole is a constant denoted by p_1 and at the other edge is zero. The principal elements of the flow are given in Refs. 21 and 22 (specifically formulas 3-34, 3-36, and 3-38): the velocity

$$v_z=-\frac{p_1}{4\mu h}(r^2-\rho^2),$$

the rate of flow

$$Q\equiv\int\int_{\text{section}}v_z dA=-\frac{\pi r^4 p_1}{8\mu h}, \tag{8}$$

and the wall shear stress

$$\tau\equiv-\mu\frac{dv_z}{d\rho}(r)=-\frac{p_1 r}{2h}. \tag{9}$$

In these formulas, the vertical pressure gradient was taken as p_1/h.

1. The direct resistance of holes

The direct resistance of the holes F_d^h is obtained by integrating the wall shear stress (9) along the boundary of the pipe. Since τ is a constant and the side area of the pipe equals $2\pi rh$ there results

$$F_d^h=-\pi r^2 p_1. \tag{10}$$

We note that the direct resistance of holes equals the force given by the pressure p_1 over the normal section area of holes.

2. The indirect resistance of holes

The change of the rim pressure to p_1 modifies the boundary condition (3) to

$$p(x,y)=p_1, \quad \text{along the rim of the hole } C_0. \tag{11}$$

It can be shown that the function

$$\hat{p}(x,y)=p(\rho)+p_1$$

with $p(\rho)$ having the expression (5), satisfies Eq. (1) and the boundary conditions (2) and (11). Consequently, the presence of the holes increases the pressure in each point of the domain D by p_1, resulting in a supplementary damping equal to to the area of the domain times the rim pressure

$$F_i^h=-p_1(d^2-\pi r^2). \tag{12}$$

3. Determination of the pressure p_1 of the rim

The pressure p_1 is obtained by equalizing the rate of flow in the pipe (8) with the volume of the incompressible fluid wd^2 leaving (or entering) the cell per unit of time as

$$p_1 = -\frac{8\mu h d^2}{\pi r^4} w.$$

Thus, in the case where the upper plate is moving up ($w > 0$), the pressure p_1 is negative and the fluid enters the planar structure.

By adding the direct hole resistance (10) with the indirect resistance (12) the total resistance of the hole for a cell is found to be

$$F^h = 8\pi\mu h\left(\frac{R}{r}\right)^4 w. \tag{13}$$

This is exactly the expression of the resistance considered in our previous papers (Refs. 16 and 17).

Remark 2: The indirect hole resistance F_i^h is larger than the direct resistance F_d^h. Therefore the disregarding of the term F_i^h cannot be justified.

C. The optimum number of holes

The area u^2 containing N cells is

$$u^2 = N\pi R^2 = Nd^2. \tag{14}$$

The total damping force over the area u^2 defined as $F^t \equiv N(F^s + F^h)$ can be written by adding the result of Eqs. (6) and (13),

$$F^t = \left\{\frac{12\mu u^4}{\pi d_0^3} C(A)\frac{1}{N} + \frac{8\pi\mu h}{A^2} N\right\} w. \tag{15}$$

Setting the derivative of F^t with respect to N equal to zero,

$$\frac{dF^t}{dN} = \left\{-\frac{12\mu u^4}{\pi d_0^3} C(A)\frac{1}{N^2} + \frac{8\pi\mu h}{A^2}\right\} w = 0,$$

gives the optimum number of holes N_{opt} as

$$N_{opt} = \sqrt{\frac{3A^2 C(A)}{2\pi^2 d_0^3 h}}\, u^2. \tag{16}$$

For this number of holes the total viscous force F^t has a minimum value. The damping coefficient is defined as the ratio of the damping force to the velocity of the plate. The corresponding minimum damping coefficient $B_{\min} \equiv F^t_{\min}/w$ is

$$B_{\min} = 8\sqrt{6}\mu \frac{\sqrt{C(A)}}{A}\sqrt{\frac{h}{d_0^3}}\, u^2. \tag{17}$$

Remark 3: The above analysis considers the area ratio, A, as a constant. This parameter can be determined by imposing other restrictions related to the plate stiffness or electrical sensitivity of the structure.

III. BASIC DESIGN FORMULAS FOR A REGULAR WEB OF ALIGNED CIRCULAR HOLES

A. The optimum number of holes on u^2 area

Formula (16) can be written as

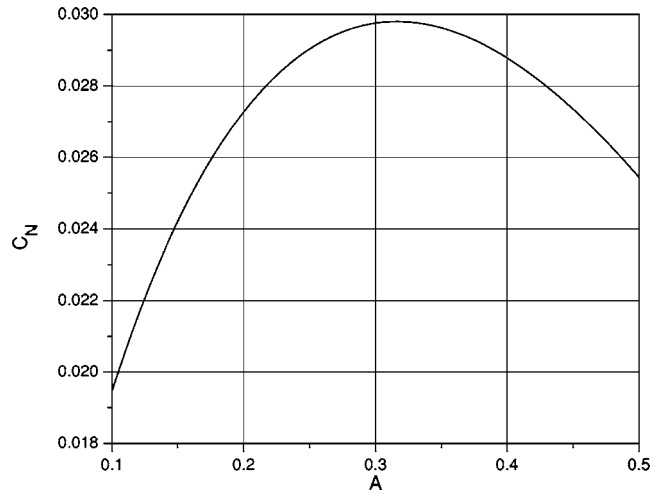

FIG. 3. The variation of the coefficient C_N with area ratio A in the case of circular holes.

$$N_{opt} = C_N \frac{u^2}{\sqrt{d_0^3 h}}, \tag{18}$$

where the coefficient C_N is

$$C_N = \sqrt{\frac{3A^2 C(A)}{2\pi^2}}. \tag{19}$$

Figure 3 gives a graph of the coefficient C_N as a function of A. The coefficient has a maximum value $C_N = 0.0298$ for $A = 0.316$. Correspondingly, the number of holes has to always be smaller than that resulting from formula (18) where the coefficient C_N has its maximum value.

B. The optimum length of the cell side

Formulas (14) and (16) give the optimum length of a side of the square cell d_{opt}

$$d_{opt} = C_d \sqrt[4]{h d_0^3}, \tag{20}$$

where the coefficient C_d has the expression

$$C_d = \sqrt[4]{\frac{2\pi^2}{3A^2 C(A)}}. \tag{21}$$

The coefficient C_d is plotted in Fig. 4. The figure shows that there is a minimum value of the cell's side length, corresponding to the same value of the area ratio $A = 0.316$, given by formula (20) where $C_d = 5.793$.

C. The optimum radius of the holes

Formulas (7), (20), and (21) provide the optimum radius of the holes as

$$r_{opt} = C_r \sqrt[4]{h d_0^3}, \tag{22}$$

where

$$C_r = \sqrt[4]{\frac{2}{3C(A)}}. \tag{23}$$

Figure 5 gives a graphical representation of the coefficient C_r as a function of A.

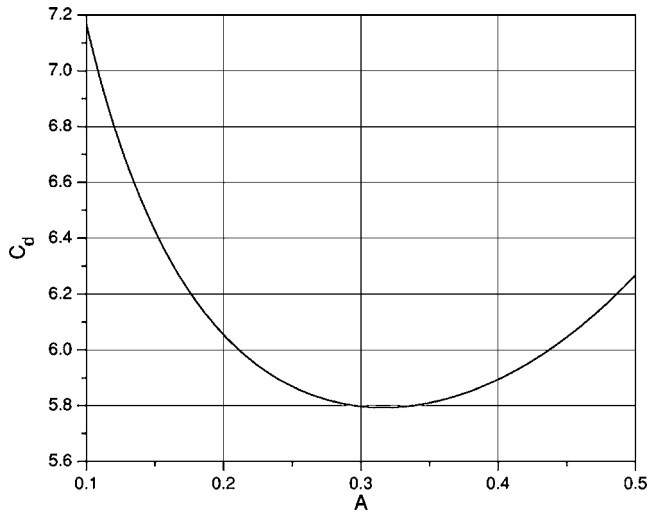

FIG. 4. The variation of the coefficient C_d with area ratio A in the case of circular holes.

D. The minimum damping coefficient

Finally, the minimum damping coefficient of Eq. (17) may be written in the form

$$B_{\min} = C_B \sqrt{\frac{h}{d_0^3}} \mu u^2, \tag{24}$$

where

$$C_B = 8\sqrt{6}\frac{\sqrt{C(A)}}{A}. \tag{25}$$

A graphical representation of the coefficient C_B is plotted in Fig. 6.

The design formulas (19), (21), (23), and (25) contain some coefficients depending only upon the area ratio. The formulas (18), (20), (22), and (24) separate the dependence on distance between the plates d_0, the thickness of the perforated plate h, and the area u^2.

Table I contains the values of these coefficients for several characteristic values of the area ratio A.

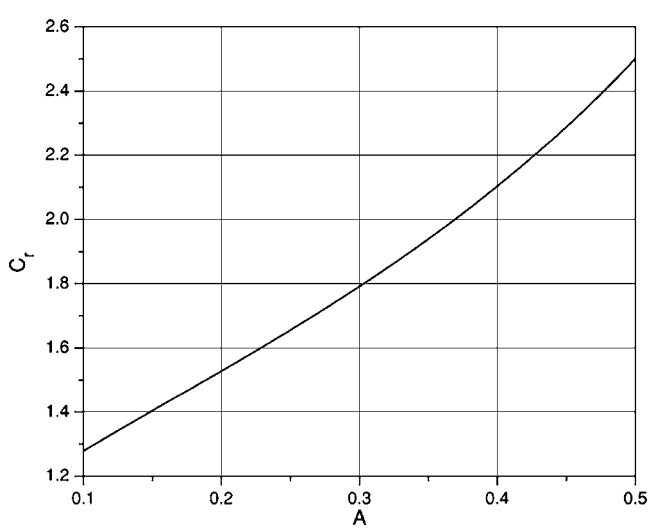

FIG. 5. The variation of the coefficient C_r with area ratio A in the case of circular holes.

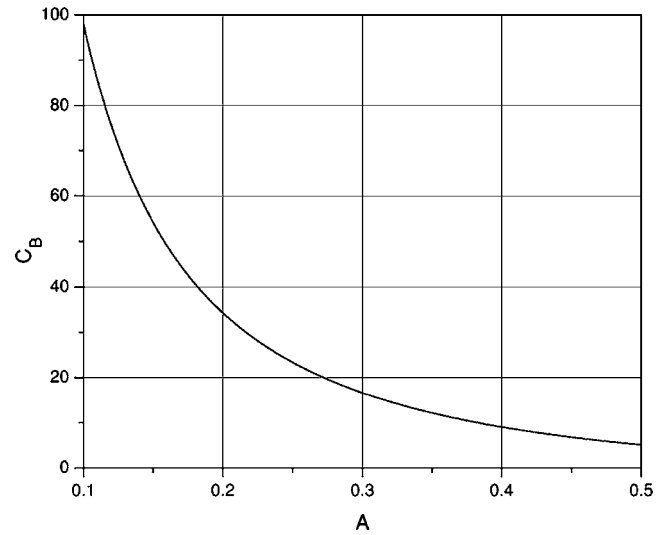

FIG. 6. The variation of the coefficient C_B with area ratio A in the case of circular holes.

Remark 4: It is possible in some cases for the value r_{opt} *to be too small to be realized technologically. If a constraint of the form*

$$r \geq r_{\min}$$

does apply, and we have $r_{\text{opt}} < r_{\min}$, *then we consider* $r_{1\text{opt}} = r_{\min}$ *and determine the other geometrical parameters by using formulas* (14) and (15). *In this case the squeeze film damping will dominate the total viscous damping.*

Remark 5: As we noted in the Introduction a certain viscous damping is needed for stabilizing the system. In the case where the minimum value of the total damping, given by formula (24), *is too low, it has to be considered again a constrained optimum value and the design parameters chosen accordingly.*

Remark 6: All the above formulas are based on modeling the squeezed film damping by Reynolds' lubrication equation. This theory applies for the viscous flow through a narrow gap between two surfaces as in Ref. 21. *In the case of less narrow gaps, the full system of Stokes equations has to be considered. Even in this case, the results obtained by applying the Reynolds' equation are conservative, the real pressure is smaller than that given by the lubrication approximation.*

IV. DESIGN FORMULAS FOR ALIGNED SQUARE HOLES

All the analysis performed in the previous section can be remade for the case where the holes are squares of $2a$ side

TABLE I. The coefficients for regular round holes.

A	$\frac{3}{4}$	$\frac{2}{3}$	$\frac{1}{2}$	$\frac{1}{3}$	$\frac{1}{4}$	$\frac{1}{5}$	$\frac{1}{6}$
C_N	0.0117	0.0167	0.0254	0.0298	0.0290	0.0273	0.0254
C_d	9.24	7.73	6.27	5.80	5.87	6.06	6.27
C_r	4.51	3.56	2.5	1.89	1.66	1.53	1.45
C_B	1.05	1.89	5.12	13.5	23.4,	34.3	46.0

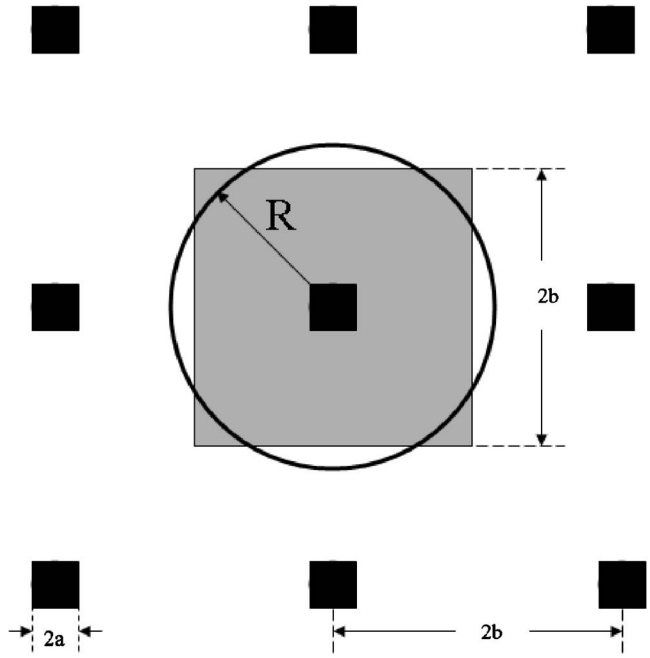

FIG. 7. The influence domain (the cell) of a square hole and its circular approximation.

lengths and the cells are also squares of $2b \equiv d$ side length (Fig. 7). We approximate the two squares with two circles of radii r and R such that

$$\pi r^2 = 4a^2, \quad \pi R^2 = 4b^2.$$

The squeezed-film damping can be written in this case as[16]

$$F_{\square}^{s} = \frac{192\mu b^4}{\pi d_0^3} C(A) w,$$

where now $A = a^2/b^2$.

The resistance of the holes can be obtained by using formula (24) given in Ref. 16 and the formula for the rate of flow for a square section given in Ref. 21,

$$F_{\square}^{h} = \frac{12}{k_1} \mu h \left(\frac{b}{a}\right)^4 w,$$

where

$$k_1 = 1 - \frac{192}{\pi^5} \sum_{j=1}^{\infty} \frac{\tanh((2j-1)\pi/2)}{(2j-1)^5} = 0.4217.$$

The total damping coefficient over area u^2 containing N cells ($u^2 = 4b^2 N$) is

$$B_{\square}^{T} \equiv F_{\square}^{T}/w = 12\mu \left[\frac{C(A)}{\pi d_0^3} \frac{u^4}{N} + \frac{1}{k_1} \frac{h}{A^2} N \right]. \tag{26}$$

This has a minimum value for

$$N_{\square opt} = \sqrt{\frac{k_1}{\pi} \frac{A^2 C(A)}{h d_0^3}} u^2. \tag{27}$$

The corresponding minimum damping coefficient is

$$B_{\square \min} = \frac{24}{\sqrt{\pi k_1}} \frac{\sqrt{C(A)}}{A} \mu \sqrt{\frac{h}{d_0^3}} u^2. \tag{28}$$

The designing formulas in this case are given in the following.

A. The optimum number of holes

We can write formula (27) as

$$N_{\square opt} = C_{\square}^{N} \frac{u^2}{\sqrt{h d_0^3}}, \tag{29}$$

where

$$C_{\square}^{N} = \sqrt{\frac{k_1}{\pi} A^2 C(A)}. \tag{30}$$

B. The optimum length of the cell side

The formula $u^2 = 4b^2 N$, combined with the relationship (27), gives the optimum cell side length as

$$d \equiv 2b_{\square \min} = C_{\square}^{b} \sqrt[4]{h d_0^3}, \tag{31}$$

where

$$C_{\square}^{b} = 1/\sqrt{C_{\square}^{N}}. \tag{32}$$

C. The optimum side length of the hole

Defining the coefficient $C_{\square}^{a}$ by the formula

$$C_{\square}^{a} = C_{\square}^{b} \sqrt{A} \tag{33}$$

and taking into account the formula $A = a^2/b^2$, the length of the side of the hole (corresponding to the minimum damping coefficient) is

$$2a_{\square \min} = C_{\square}^{a} \sqrt[4]{h d_0^3}. \tag{34}$$

D. The minimum damping coefficient

The minimum damping coefficient (28) can be written as

$$B_{\square \min} = C_{\square}^{b} \sqrt{\frac{h}{d_0^3}} \mu u^2, \tag{35}$$

where

$$C_{\square}^{b} = \frac{24}{\sqrt{\pi k_1}} \frac{\sqrt{C(A)}}{A}. \tag{36}$$

Remark 7: We have

$$\frac{C_{\square}^{b}}{C_b} = \frac{24}{8\sqrt{6}\sqrt{\pi k_1}} = 1.064.$$

Therefore the damping coefficient in the case of circular holes is smaller than that corresponding to the case of square holes, but the difference is so small that square and round holes can be considered in many cases to be practically equivalent.

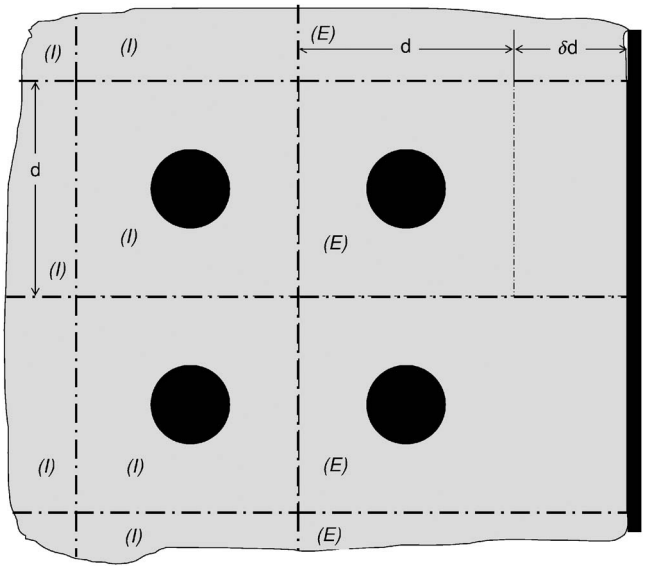

FIG. 8. The edge "E" and the inner "I" cells.

V. THE EDGE CORRECTION IN DESIGNING PERFORATED PLANAR MICROSTRUCTURES

The analysis in the previous sections assumed the perforated planar microstructure to be infinite in both the Ox and Oy directions. A real structure is, of course, finite having several edges. The Neumann boundary condition satisfied on a closed side of the domain, $\partial p/\partial n=0$, is compatible with the condition on the external curve of the cell. Consequently the closed sides of the domain boundary do not need any correction. The boundary condition on an open side of the boundary is of Dirichlet type ($p=0$), different from the Neumann condition required by the external curve of the cell. This gives a pressure change from cell to cell that breaks the periodicity of the flow and results in an additional squeezed-film flow component from the center of the microstructure towards the open edges. In order to obtain a better design of such a structure we have to include corrections due to the open structure edges.

A. The edge correction

Figure 8 shows a part of a perforated planar microstructure including some edge cells (denoted by (**E**)] and also the neighbors inside cells [denoted by (**I**)]. Correspondingly, the pressure function in an edge cell will be denoted by $p^{(E)}(x,y)$ while the same function corresponding to an inner cell will receive the superscript $(I):p^{(I)}(x,y)$. The main difference in analyzing the two types of cells is that while for (**I**)-cells the boundary condition along all rectilinear sides $\mathcal{C}_N^I$ (represented by dotted lines in Fig. 8) is of the Neumann homogenous type, for the edge cells the boundary condition along the external side of the cell, denoted by $\mathcal{C}_D^E$, requiring the canceling of the pressure, is of Dirichlet type; along the remaining external curve of the (**E**) cell's boundary $\mathcal{C}_N^E$ (dotted lines in Fig. 8) the condition is, again, of Neumann homogeneous type. Physically, this condition will give a smaller value for the total pressure of a square (**E**) cell as compared with that corresponding to an inner cell. In order

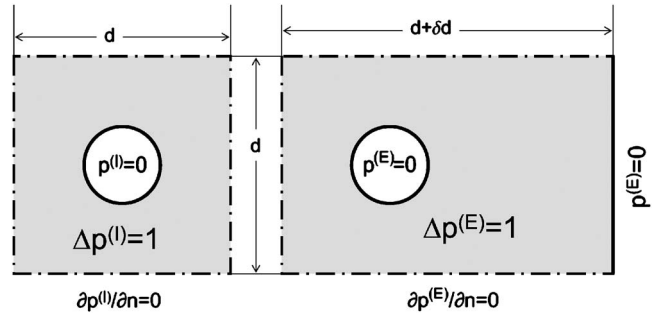

FIG. 9. The boundary-value problems corresponding to an "edge" and to an "inner" cell.

to increase the total pressure of an edge cell we increase the length of its sides perpendicular to the plate edge by a value δd. The value of this parameter is obtained from the condition that the total pressure resulting from the squeezed-film damping for the modified edge cell be equal to the total pressure corresponding to an inner cell. This increase of the total pressure of the open edge cells will result in a supplementary squeezed-film flow component, towards the center of the damper, which cancels the additional squeezed film component.

Mathematically we consider the canonical boundary-value problems (Ref. 17) for the two types of cells

$$\Delta p^{(I)}(x,y)=1 \text{ in } \mathcal{D}^{(I)}, \quad p^{(I)}|_{\mathcal{C}_0^I}=0, \quad \left.\frac{\partial p^{(I)}}{\partial n}\right|_{\mathcal{C}_N^I}=0, \tag{37}$$

$$\Delta p^{(E)}(x,y)=1 \text{ in } \mathcal{D}^{(E)}, \quad p^{(E)}|_{\mathcal{C}_0^E\cup\mathcal{C}_D^E}=0,$$

$$\left.\frac{\partial p^{(I)}}{\partial n}\right|_{\mathcal{C}_N^E}=0. \tag{38}$$

Here $\mathcal{D}^{(I)}$ and $\mathcal{D}^{(E)}$ are the domains corresponding to an inner and edge cell, respectively, and $\mathcal{C}^0$ and $\mathcal{C}_0^E$ denote the central circles in both cases (Fig. 9). The parameter δd results by solving the equation

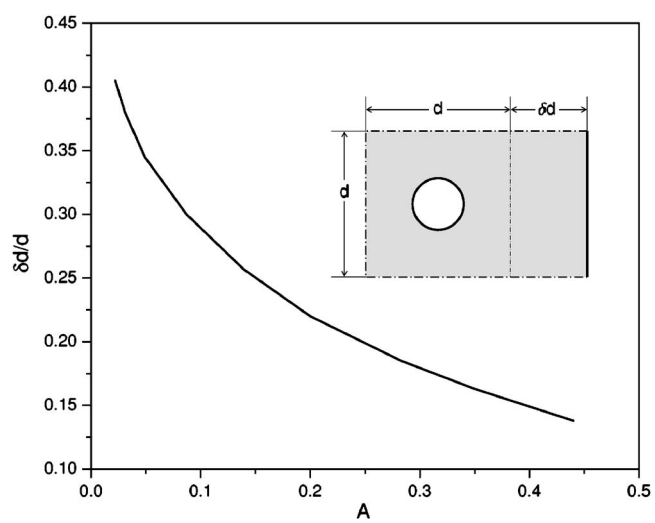

FIG. 10. The variation of the ratio $\delta d/d$ with area ratio A.

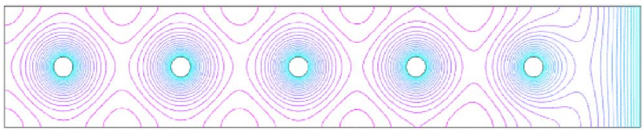

FIG. 11. (Color online) The pressure graph for a damper with five holes and with an opened right side.

$$P^{(I)} \equiv \int\int_{\mathcal{D}^I} p^{(I)}(x,y)\,dx\,dy = \int\int_{\mathcal{D}^E} p^{(E)}(x,y)\,dx\,dy \equiv P^{(E)}. \tag{39}$$

It is clear that the geometry of the problem changes with the area ratio of the domain. Consequently, the correction δd depends upon the area ratio A. This is why Eq. (39) has to be solved for each value of this parameter. We have determined the solutions of the two boundary-value problems (37) and (38), for area ratio values in the range of practical interest, by using the Partial Differential Equation (PDE) Toolbox and its associated graphical user interface (GUI) of MATLAB. Finally, we have solved Eq. (39) for each value of the area ratio by a bisection-type technique. The results are plotted in Fig. 10.

Thus the edge correction consists of increasing the sides of the edge cells (perpendicular to the edge line) by the value δd. This is the same as decreasing the domain containing uniformly spaced circular holes with the value δd for all the open sides of the physical domain parallel to the coordinate axis, and considering the design problem for the resulting domain. It can result in eliminating a line or/and a column of holes in some cases.

B. Numerical validation of the open edge correction

In order to validate the proposed correction to the open side boundaries we consider a domain with one-dimensional periodicity in the y direction, a closed side on the left, and an open side to the right. In dimensionless variables we consider the canonical boundary-value problem, which gives the Poisson' equation for the pressure

$$\Delta p(x,y) = 1$$

in the multiconnected domain consisting of a line of cells with homogeneous Neumann-type boundary conditions on the upper, lower, and left boundaries and with Dirichlet homogeneous conditions on the right (open) side and on the rim of holes. The dimensions of the open edge cell were modified according to the results in Fig. 10. Since the additional squeezed-film flow component is more important for small values of A numbers, we have chosen $d=1$, $r=0.084$.

TABLE II. The error after edge correction in the case $A=0.022$.

j	P_j	$\tilde{P}_j = j \star P_1$	ϵ_j
1	0.189 692	0.189 692	0
2	0.379 217	0.379 384	$4.\times 10^{-4}$
3	0.568 906	0.569 076	$3.\times 10^{-4}$
4	0.758 598	0.758 768	2.2×10^{-4}
5	0.948 291	0.948 460	1.8×10^{-4}

Hence there results $A=0.022$, $\delta d=0.405$. Due to similarity of the PDE equation and of the boundary conditions we have used the COMSOL software for the steady state heat conduction problem (which is a finite element implementation). The graph of the pressure, given in Fig. 11, shows qualitatively the periodicity of the pressure in the cells next to the end cells. We computed the total pressure P_j, $(j=1,2,\ldots,5)$ for the model domain having j cells. The total pressure given by our edge correction will be $\tilde{P}_j = j \star P_1$, $(j=1,2,\ldots,5)$. The results are given in Table II, where ε_j is the relative error.

Due to the way the boundary condition was defined, an open edge cell and the cell next to it have the same total pressure. However, ϵ_2 is not zero due to the fact that the roots of Eq. (39) were computed with several valid digits (three in this example). It is to be noticed that $\epsilon_2 > \epsilon_3 > \epsilon_4 > \epsilon_5$, indicating that the edge effect is diminishing with the distance to the microstructure edge.

For more validation of the edge correction for open boundaries we considered the simulations included in Table III covering all the range of area ratio A considered in the graph in Fig. 10.

The error in the second column is connected with the precision of the determination of the root of Eq. (39) and also the precision of the Finite Element Program for solving the corresponding BVP. The largest error introduced by our model of the edge correction is smaller than 0.04%. These simulations show that the proposed edge correction works very well validating the adopted model.

The edge correction presented here works in the case of perforated structures with unidimensional symmetry. It is clear that it is not working for the "*corner*" cells, which need separate analysis. The external geometry of a corner cell is completely determined by the geometry of the adjacent sides. This is why the only parameter that can be used for equalizing the total pressure of a corner cell with that corresponding to an inner cell is the radius of the hole. Consequently, the corner correction adjusts the radii of the corner holes. Generally, the number of corner cells is low compared with the total number of holes of a given microstructure. This is why

TABLE III. The error after edge correction for $A=0.022-0.44$.

A	r	δd	ϵ_2	ϵ_3	ϵ_4	ϵ_5
0.022	0.084	0.405	4.0×10^{-4}	3.0×10^{-4}	2.2×10^{-4}	1.8×10^{-4}
0.031	0.1	0.38	5.2×10^{-5}	3.9×10^{-5}	2.9×10^{-5}	2.3×10^{-5}
0.139	0.21	0.257	1.0×10^{-4}	7.0×10^{-5}	5.0×10^{-5}	4.0×10^{-5}
0.283	0.3	0.1855	$<10^{-6}$	$<10^{-6}$	$<10^{-6}$	$<10^{-6}$
0.44	0.374	0.138	$<10^{-6}$	$<10^{-6}$	2.5×10^{-5}	1.8×10^{-5}

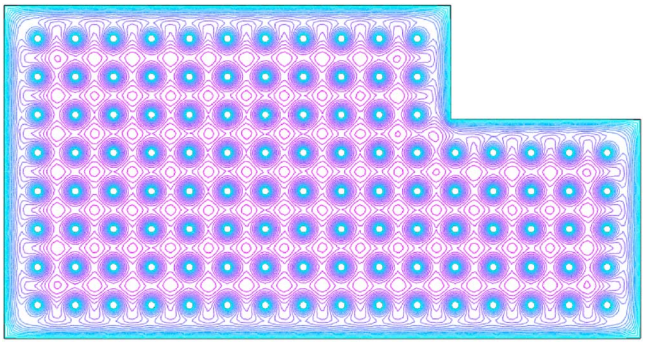

FIG. 12. (Color online) The pressure graph for a microstructural damper containing 113 holes, a reentrant corner, and five external corners.

the corner adjustments are less important than the side corrections.

The microstructure in Fig. 12 has 113 holes, five external corners, and one reentrant corner. All the sides are open such that the edge correction was applied to all of them. The total pressure obtained by using a FEM code for the whole structure equals $TP=18.460$. The total pressure for an inner cell is $TP^{(I)}=0.1629$ and hence the approximation for the whole structure equals $\widetilde{TP}=113\times TP^{(I)}=18.408$. The relative error is $\varepsilon=0.28\%$. The total pressure for the whole structure without applying the edge correction, obtained again by using a FEM code, is $TP'=15.017$. Thus, if the edge correction was not applied, the relative error for the whole structure would have been $\varepsilon'=18\%$. We also note that the smallness of the error after applying the edge correction makes it unnecessary to apply the corner corrections.

VI. SPECIAL CORRECTIONS TO THE BASIC DESIGNING FORMULAS

In this section various corrections are discussed for the design formulas, taking into consideration the rarefied gas effect, effect of the ends of the hole, compressibility of the gas, and inertia. All the corrections will be considered for the case of circular holes.

A. Corrections due to the rarefied gas effects

It has been shown in Refs. 23 and 17 that at small air gaps, when the molecular mean free path λ' is not negligible compared with the gap width d_0, which is the case in many perforated planar microstructures, the rare gas effects become important. In this case formula (6) still holds if the viscosity coefficient μ is replaced by the effective viscosity μ':

$$\mu' = \frac{\mu}{1+6\sigma_P K_n'}.$$

The Knudsen number $K_n'=\lambda/d_0$ includes the slip correction due to the flow profile for a rare gas. For a diffuse scattering model $\sigma_P=1.016$ and the molecular mean free path λ can be calculated via the pressure P, the temperature T, the shear viscosity μ, and the molecular mass m (Ref. 24),

$$\lambda = \frac{\sqrt{\pi}\mu}{2P}\left(\frac{2k_BT}{m}\right)^{1/2},$$

where $k_B=1.380658\times 10^{-23}$ J/K is Boltzmann's constant.

On the other hand, if the holes are very thin (*Knudsen number* $K_n''=\lambda/r$ is large), the slip boundary condition has to be again considered in the capillaries. The resistance of the flow in holes can still be determined by using formula (13) if the effective viscosity μ''

$$\mu'' = \frac{\mu}{1+4\sigma_P K_n''},$$

is taken to be the viscosity coefficient.

Consequently, formula (16) includes a correction factor c for rarefaction

$$c = \sqrt{\frac{\mu'}{\mu''}},$$

and in formula (17) the viscosity coefficient is substituted by the geometrical average

$$\mu \to \sqrt{\mu'\mu''}.$$

Correspondingly, formula (18) has c as a factor on the right-hand side and the right-hand side terms in formulas (20) and (22) have to be divided by $\sqrt{c}$. Finally, in formula (24) $\sqrt{\mu'\mu''}$ has to be substituted for the viscosity coefficient μ.

B. The correction for the hole end effect

The fully developed Poiseuille flow, assumed in the calculations of the resistance of holes in Eq. (13), theoretically holds only for infinite ducts. In the case where the thickness of the plate h and the radius r are of comparable dimensions a correction has to be made for the effect of the finite length of holes. Shapirov and Seleznev in Ref. 24 have shown that this effect can be included in formula (13) by replacing the length of holes with

$$h_{\text{eff}} = h + \frac{3\pi r}{8}.$$

Correspondingly, in all the basic design formulas the effective length h_{eff} will be used instead of the depth into the page h.

C. Correction to Skvor's model

The derivation of the basic designing formulas was based on approximating the cell with a circular domain shown in Fig 2. The error resulting from this assumption was analyzed in Ref. 17, Sec. VII. The results show that Skvor's approximation works well for $A<0.4$. For larger values of the area ratio, A, a corrected formula

$$C^*(A) = C(A) + 10^{-4}(8.7 - 10\sqrt{A} + 26A - 27A\sqrt{A})$$

can be used instead of Skvor's function $C(A)$. This correction extends the applicability of the analytical approach up to $A=0.75$.

D. Corrections for higher frequencies

The analysis presented here holds, true in the range of audible acoustical frequencies. For higher frequencies, the effects of inertia and compressibility become important. The coefficients accounting for the combined influence of inertia and compressibility can be determined by using the formulas given in Ref. 17, Sec. IV.

VII. EXAMPLE OF APPLICATION OF GIVEN FORMULAS

As an application we consider the backplate of a high sensitivity MEMS microphone designed by Hsu *et al.* in Ref. 25 and analyzed also in Ref. 26. The backplate has a square geometry with the side length of $L=2580$ μm, the gap underneath is $d_0=4$ μm, and the thickness $h=13$ μm. The backplate has a periodic system of 441 square holes of area 60×60 μm^2. The area ratio is

$$A = (441 \times 60^2/2580^2) = 0.2385.$$

The total damping coefficient for this perforated plate can be determined by using Eq. (26) where $\mu_{air}=1.846 \times 10^{-5}$ [kg/(m s)]. We obtain

$$B^{old} = 1.06 \times 10^{-2} \text{ (Ns/m)}.$$

A. Redesign the microstructure with square holes

We can redesign this planar microstructure such that the resulting device has square holes and a minimum damping coefficient. In this case formulas (29)–(36) give

$$N_{\square\text{opt}} = 6230, \quad 2b = 32.7 \ (\mu\text{m}),$$

$$2a = 16 \ (\mu\text{m}), \quad B_{\square\text{min}} = 1.48 \times 10^{-3} \text{ (Ns/m)}.$$

B. Redesign the structure with circular holes

In the case where we use circular holes instead of square perforations, the design data given by formulas (18)–(25) are

$$N_{\text{opt}} = 6630, \quad d = 31.7 \ (\mu\text{m}), \quad r = 8.7 \ (\mu\text{m}),$$

$$B_{\text{min}} = 1.4 \times 10^{-3} \text{ (Ns/m)}.$$

This way the redesign of the perforated microstructure resulted in a reduction of the damping coefficient by a factor of 7 in the case of square holes and by a factor of 7.6 when circular holes are used.

C. Application of the edge correction

In order to apply the edge correction we note that for $A=0.24$, as given above, the graph in Fig. 10 gives $\delta d/d=0.2$ and hence $\delta d=6.4$ (μm) for each side of the rectangle. Applying this correction to all sides, the reduced domain has the sides of dimensions equal to $\tilde{L}=2567$ (μm). Correspondingly, we obtain a number of $N_1=81$ cells along each side of the backplate. This gives a total of 6561 cells. The final design data are

$$d = 31.7 \ (\mu\text{m}), \quad r = 8.7 \ (\mu\text{m}), \quad N_1 = 81,$$

the central cell being in the center of the given square.

Let us now suppose that we have a technological restriction of $r \geq 20$ μm. In this case the formula (7) gives

$$d = \sqrt{\frac{\pi}{A}} r = 35.5 \ (\mu\text{m})$$

and hence

$$N_1 = \frac{\tilde{L}}{d} = 35; \quad N = N_1^2 = 1225 \text{ holes}.$$

Correspondingly, the damping coefficient, obtained by dividing the result of Eq. (15) by the velocity w, is

$$B' = 3.9 \times 10^{-3} \text{ (Ns/m)}.$$

This way we obtain a reduction of the total damping of a factor of almost 3 as compared with the initial design for the same area ratio.

D. Application of the rarefied gas and hole end effect corrections

The parameters for the air at atmospheric pressure used in the calculations are the pressure $P=101.3\times 10^3$ (N/m^2), the temperature $T=300$ K, viscosity $\mu=1.85 \times 10^{-5}$ (Ns/m^2), and mean free path $\lambda=68.2\times 10^{-9}$ (m).

The results, after applying the *rarefied gas effect* correction and and the correction for the *effect of the ends of holes*, are

$$N_{\text{opt}} = 8572, \quad d = 28.3 \ (\mu\text{m}), \quad r = 6.7 \ (\mu\text{m}),$$

$$B_{\text{min}} = 1.3 \times 10^{-3} \text{ (Ns/m)}.$$

By also adding the edge correction the design data become

$$d = 28.3 \ (\mu\text{m}), \quad r = 6.7 \ (\mu\text{m}), \quad N_1 = 91.$$

VIII. CONCLUSIONS

(a) The formula for the optimal number of holes provides the smallest damping coefficient for the given area ratio.
(b) In all of the results presented here, the dependence on the area ratio is separated from the dependence on the other parameters of the problem.
(c) The effect of the side correction can be easily incorporated into analyses by reducing the domain occupied by holes by δd for each open side of the domain.
(d) It is shown (see Fig. 6) that the damping coefficient is strongly dependent on area ratio of the plate: when the area ratio is increased the damping coefficient decreases significantly. However, removing more material from the plate reduces the stiffness of the plate and also decreases its mass. Also, in some applications the (electrical) sensitivity of the system is directly correlated with the area ratio of the perforated plates. Since these elements are

basic properties it is important to find a proper balance between the removed portion (area ratio) and the damping coefficient.

(e) The analysis in Sec. II shows that the *indirect resistance of holes* is more important than the *direct resistance*.

ACKNOWLEDGMENTS

This work has been supported through NIH Grant No. R01 DC05762-1A1 to RNM.

[1]T. B. Gabrielson, "Mechanical-thermal noise in micromachined acoustic and vibration sensors," IEEE Trans. Electron Devices, **40**, 903–909 (1993).

[2]M. Gad-el-Hak (ed.), *MEMS Applications* (CRC Press, Taylor & Francis Group, Boca Raton, FL, 2006).

[3]M-H. Bao, *Micro Mechanical Transducers* (Elsevier, Amsterdam, 2000).

[4]H. M. Saad and A. K. Stiffler, "Squeeze film dampers amplitude effects at low squeeze numbers," J. Eng. Ind. **97**, 1366–1370 (1975).

[5]J. B. Starr, "Sqeeze-film damping in solid-state accelerometers," Tech. Digest IEEE Solid State Sensor and Actuator Workshop, Hilton Head Island, SC, June 1990, pp. 44–47.

[6]Y. J. Yang and S. D. Senturia, "Numerical simulation of compressible squeezed-film damping," Tech. Digest IEEE Solid State Sensor and Actuator Workshop, Hilton Head Island, SC, June 1990, pp. 76–79.

[7]A. H. Nayfeh and M. I. Younis, "A new approach to the modeling and simulation of flexible microstructures under the effect of squeeze-film damping," J. Micromech. Microeng. **14**, 170–181 (2004).

[8]T. Veijola, K. Ruokonen, and Tittonen, "Compact model for squeezed-film damping including the open border effects," in *Proceedings of MSM 2001*, Hilton Head SC, 19–21 March, 2001, pp. 76–79.

[9]T. Veijola, "Analytic Damping Model for an MEM Perforation Cell," Microfluid. Nanofluid. **2**(3), 249–260 (2006).

[10]T. Veijola and T. Mattila, "Compact squeezed-film damping model for perforated surface," in *Proc. Transducers '01*, München, Germany, 10–14 June 2001, pp. 1506–1509.

[11]P. Raback, A. Pursula, V. Junttila, and T. Veijola, "Hierarchical finite element simulation of perforated plates with arbitrary hole geometry," in *Proceedings of the 6th International Conference on Modeling and Simulation of Microsystems*, San Francisco, 2003, Vol. 1, pp. 194–197.

[12]Y.-J. Yang and C.-J. Yu, "Macromodel extraction of gas damping effects for perforated surfaces with arbitrary-shaped geometrics," in *Proceedings of the 5th International Conference on Modeling and Simulation of Microsystems*, San Juan, 2002, pp. 178–181.

[13]T. Veijola and P. Raback, "A method for solving arbitrary mems perforation problems with rare gas effects," in *Proceedings of the 8th International Conference on Modeling and Simulation of Microsystems*, NSTI-Nanotech 2005, Anaheim, Vol. 3, pp. 561–564.

[14]M. Bao, H. Yang, Y. Sun, and P. J. French, "Modified Reynolds, equation and analytical analysis of squeeze-film air damping of perforated structures," J. Micromech. Microeng. **13**, pp. 795–800 (2003).

[15]M. Bao, H. Yang, Y. Sun, and Y. Wang, "Squeeze-film air damping of thick hole-plate," Sens. Actuators, A, **A108**, 212–217 (2003).

[16]D. Homentcovschi and R. N. Miles, "Modelling of viscous damping of perforated planar micromechanical structures. Applications in acoustics," J. Acoust. Soc. Am. **116**(5), 2939–2947 (2004).

[17]D. Homentcovschi and R. N. Miles, "Viscous Damping of Perforated Planar Micromechanical Structures," Sens. Actuators, A **A119**, 544–552 (2005).

[18]A. J. Zuckerwar, "Theoretical response of condenser microphones," J. Acoust. Soc. Am. **64**, 1278–1285 (1978).

[19]C. W. Tan and J. Miao, "Analytical modeling for bulk-micromachined condenser microphones," J. Acoust. Soc. Am. **120**(2), 750–761 (2006).

[20]Z. Ščvor, "On acoustical resistance due to viscous losses in the air gap of electrostatic transducers," Acustica **19**, 295–297 (1967-1968).

[21]F. M. White, *Viscous Fluid Flow* (McGraw-Hill, New York, 1992).

[22]H. Ockendon and J. R. Ockendon, *Viscous Flow* (Cambridge U.P., Cambridge, 1995).

[23]T. Veijola, H. Kuisma, J. Lahdenperä, and T. Ryhänen, "Equivalent-circuit model of the squeezed gas film in a silicon accelerometer," Sens. Actuators, A **A48**, 239–248 (1995).

[24]M. H. Shapirov and V. Seleznev, "Data on internal rarefied gas flows," J. Phys. Chem. Ref. Data **27**, 657–706 (1997).

[25]P. C. Hsu, C. H. Mastrangelo, and K. D. Wise, "A high sensitivity polysilicon diaphragm condenser microphone," Digest Workshop on MicroElectroMech. Systems (MEMS), Heidelberg, January 1998, pp. 580–585.

[26]S. S. Mohite, V. H. Kesari, R. Sonti, and R. Pratap, "Analytical Solutions for the Stiffness and Damping Coefficients of Squeeze Films in MEMS Devices having Perforated Back Plates," J. Micromech. Microeng. **15**, 2083–2092 (2005).